Thin Solid Films 529 (2013) 200–204

Contents lists available at SciVerse ScienceDirect

Thin Solid Films

journal homepage: www.elsevier.com/locate/tsf

Resistive switching characteristics of gallium oxide for nonvolatile memory application

Jyun-Bao Yang [b], Ting-Chang Chang [a,b,*], Jheng-Jie Huang [a], Shih-Ching Chen [a], Po-Chun Yang [b], Yu-Ting Chen [b], Hsueh-Chih Tseng [a], Simon M. Sze [c], Ann-Kuo Chu [b], Ming-Jinn Tsai [d]

[a] Department of Physics, National Sun Yat-Sen University, Kaohsiung, Taiwan
[b] Department of Photonics, National Sun Yat-Sen University, Kaohsiung, Taiwan
[c] Institute of Electronics, National Chiao Tung University, Hsin-Chu, Taiwan
[d] Electronics and Optoelectronics Research Laboratory, Industrial Technology Research Institute, Chutung, Hsinchu, Taiwan

A R T I C L E I N F O

Available online 25 October 2012

Keywords:
RRAM
Gallium oxide
Oxygen vacancies

A B S T R A C T

This study investigates bipolar resistance switching memory in a fabricated Pt/GaO_x/TiN device. Gallium oxide sputtered in ambient Ar shows a change in resistance ratio of two orders of magnitude. The enhancement of resistance ratio is also observed in the gallium oxide layer when deposited in ambient Ar/O_2. The X-ray photoelectron spectroscopy analysis shows that this gallium oxide in ambient Ar/O_2 can reduce the number of defects and enhance the stability of switching behavior. An analysis of current transport mechanism in the high resistance state indicates that the larger effective thickness can be attributed to the higher oxygen concentration, and can increase the resistance value of the high resistance state.

© 2012 Elsevier B.V. All rights reserved.

1. Introduction

Recently, the development of nonvolatile memory has been influenced by device dimension scaling. When devices are continuously miniaturized, the tunneling oxide of the floating-gate memory will become thinner [1]. Consequently, the stored charges can leak back to the substrate and lead to a loss of stored information [2–5]. In order to solve this problem, the next generation non-volatile memories must be developed, such as ferroelectric random access memory [6], magnetic random access memory [7], phase change random access memory [8], and resistance random access memory (RRAM) [9]. RRAM has attracted considerable interest due to its advantages of simple structure, low energy consumption, higher operating speed and higher endurance [10–14]. Therefore, many studies of promising materials have been reported, such as organic materials [15] and transition metal oxides [16–21].

2. Experiment

The substrate used in this experiment was TiN/SiO_2/Si, with the 200-nm-thick SiO_2 (low temperature oxide, LTO) deposited on the TiN. Moreover, we defined the size of via (4×4 μm) by etching the LTO layer. Secondly, a 23-nm-thick GaO_x insulator layer was deposited on the previous substrate by sputtering a $Ga_{0.4}O_{0.6}$ target at room temperature in ambient Ar (30 sccm), and labeled as sample A. In addition, a 22.7-nm-thick GaO_x was also deposited on the substrate in Ar/O_2 (30 sccm/10 sccm) for comparison as sample B. The sputtering power, deposition rate and working pressure were set to 150 W, 23 Å/min and 0.53 Pa, respectively. Finally, the Pt/GaO_x/TiN device was completed by capping the top electrode (Pt) on the GaO_x shown in the inset of Fig. 1. The resistive switching characteristics of Pt/GaO_x/TiN were measured by an Agilent B1500 semiconductor

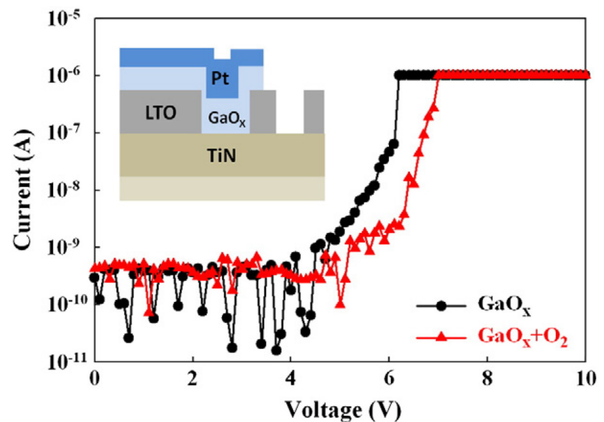

Fig. 1. The forming process of samples A and B. Inset is the Pt/GaO_x/TiN device schematic diagram.

* Corresponding author at: Department of Physics, National Sun Yat-Sen University, Kaohsiung, Taiwan. Tel.: +886 7 5252000 3708; fax: +886 7 5253709.
E-mail address: tcchang@mail.phys.nsysu.edu.tw (T.-C. Chang).

0040-6090/$ – see front matter © 2012 Elsevier B.V. All rights reserved.
http://dx.doi.org/10.1016/j.tsf.2012.10.026

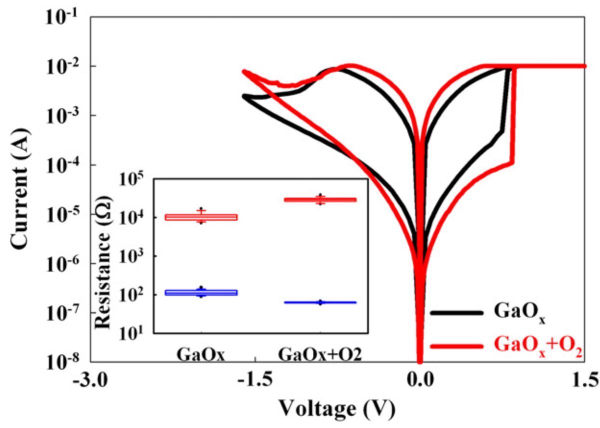

Fig. 2. The bipolar switching characteristics of samples A and B. Inset is the 100 cycle endurance characteristic, which is swept by DC voltage.

parameter analyzer, and the composition of the gallium oxide film was analyzed by X-ray photoelectron spectroscopy (XPS, JEOL JPS 9010 MX). The spectrometer source of Al Kα (1486.6 eV) radiation was used for XPS analysis. All of the peaks shape and parameters were fitting by using the software of XPSPEAK (Version 4.1) with Lorentzian–Gaussian functions. In addition, before gathering the XPS signal, the sample surface had been cleaning by argon ions beam. The beam voltage and beam current were 500 V and 8 mA, respectively.

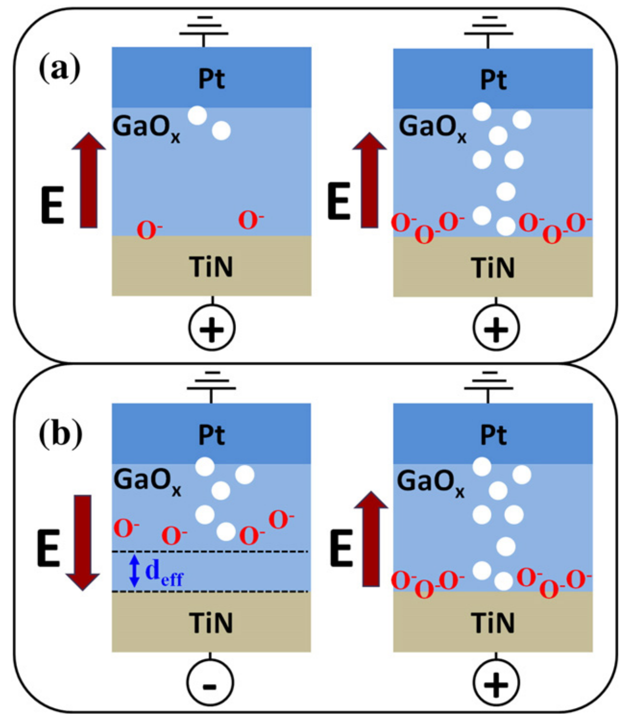

Fig. 4. The resistance switching mechanism of Pt/GaO_x/TiN during (a) the forming process and (b) the set and reset process.

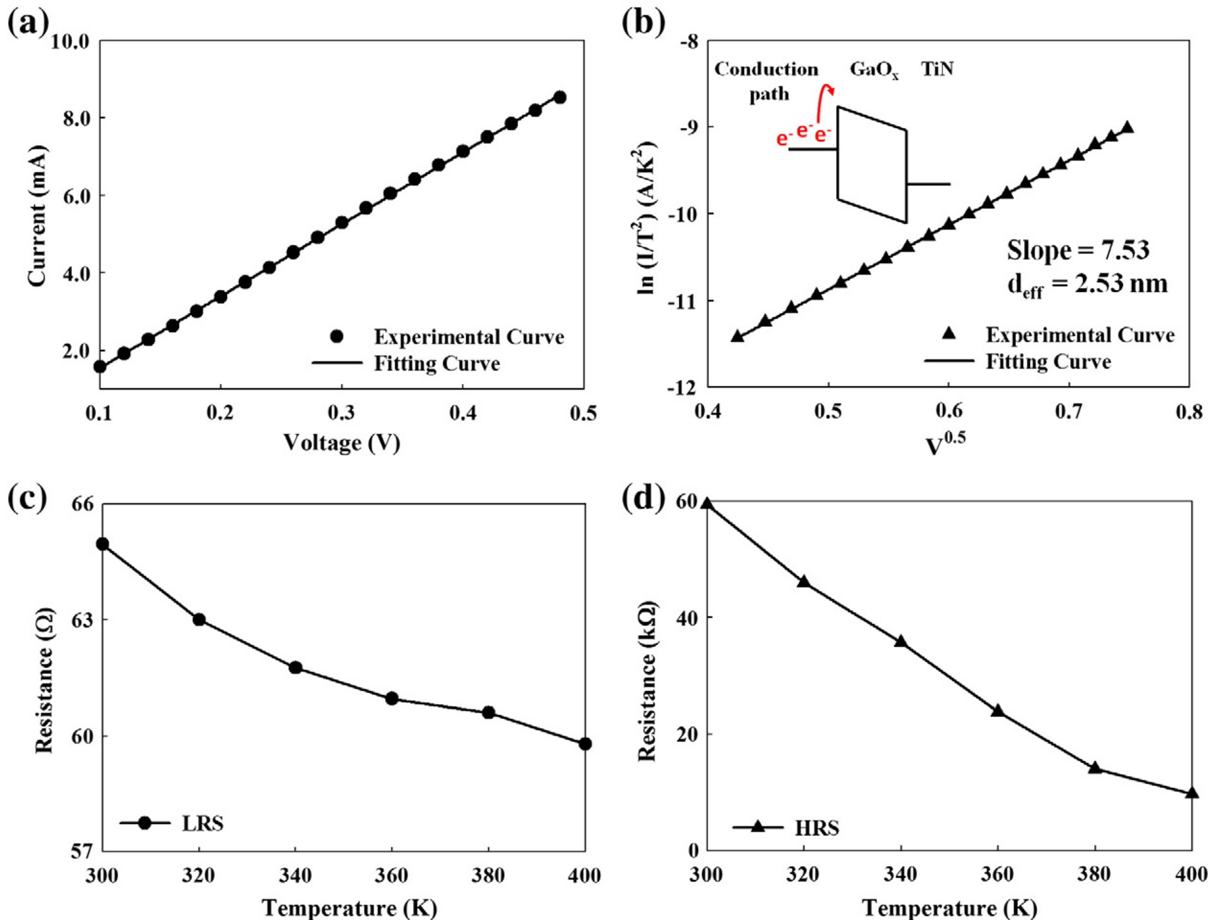

Fig. 3. The current transport models for sample B for (a) Ohmic conduction and (b) Schottky emission. The resistance values of (c) LRS and (d) HRS are observed at temperatures ranging from 300 K to 400 K.

Fig. 5. XPS analysis of (a) O 1s for sample A, (b) O 1s for sample B, (c) Ga $3d_{5/2}$ for sample A and (d) Ga $3d_{5/2}$ for sample B.

3. Results and discussion

In this work, the voltage was applied on the TiN electrode and the Pt electrode was grounded. A +10 V was applied with a current compliance of 1 μA on both samples A and B for the purpose of device activation, namely the forming process. The voltage where the current increases abruptly is defined as the forming voltage. Fig. 1 shows that the forming voltage of sample A (6.2 V) is lower than that of sample B (7 V). Since the conduction paths are constructed during the forming process, the resistance state is switched to low resistance state (LRS). By sweeping voltage from 0 V to −1.6 V, the resistance state is switched from LRS to high resistance state (HRS), named reset process. Subsequently, the set process is employed to switch the LRS by sweeping from 0 V to 2 V with a current compliance of 10 mA.

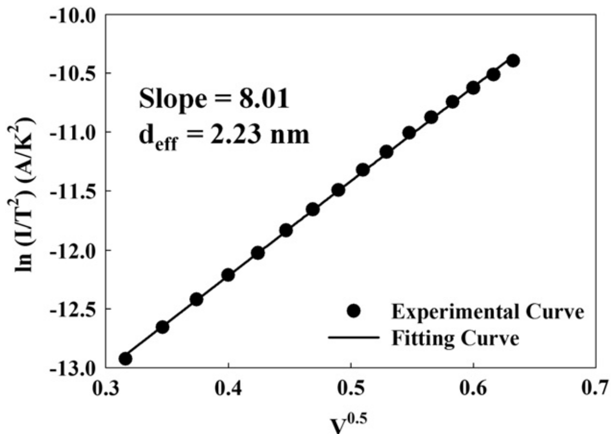

Fig. 6. The current transport models of Schottky emission for sample A.

Fig. 2 shows the resistive switching behavior of the gallium oxide film. The resistance ratio extracted at 0.2 V is approximately 2 orders of magnitude for sample A (in black), and is enhanced to about 2.5 orders for sample B (in red), as shown in Fig. 2 and its inset. Through this statistical comparison, the switching behavior of sample B can be clearly seen as being more stable.

In order to investigate the resistive switching behavior, the carrier transport mechanisms are analyzed. The analysis result indicates that the current of sample B is dominated by Ohmic conduction and by Schottky emission in LRS and HRS, respectively, as shown in Fig. 3(a) and (b). When the device is switched to HRS, the gallium oxide film conduction path ruptures and the switching layer is formed. When voltage is applied to the TiN electrode, the electrons in the conduction path acquire enough energy to overcome the barrier height between the Fermi level of the conduction path and the GaO_x conduction band, as shown in the inset of Fig. 3(b). Moreover, the carrier transport mechanisms of sample A are similar to that of sample B. In order to study the resistance switching mechanisms, the resistance variation trends for LRS and HRS are observed at temperatures ranging from 300 K to 400 K. The decreasing resistance value of LRS with the rising temperature indicates that conduction paths have a semiconductor-like (oxygen vacancies) property [23], as shown in Fig. 3(c). Furthermore, the conduction mechanism can be confirmed to be the Schottky emission

from the decreasing resistance in HRS while temperature rises, as shown in Fig. 3(d).

According to the analysis above, we can conclude that the current transport mechanism of the Pt/GaO_x/TiN structure is related to oxygen vacancies [22,23], and a model responsible for the conduction mechanism is therefore proposed. Fig. 4 shows the resistance switching behaviors of the Pt/GaO_x/TiN structure. During the forming process, when applying a positive voltage on the TiN electrode, the oxygen vacancy conduction path is formed due to the break of the Ga–O bonds by high energy electrons, as shown in Fig. 4(a). Subsequently, the oxygen ions migrate toward the TiN because of the electric-field direction and are reserved in the TiN electrode. When a negative bias is applied, the oxygen ions move away from the TiN/GaO_x interface and re-combine with the oxygen vacancies along the conduction path. As a result, the resistance value is switched to HRS because the switching layer is formed between TiN and the conduction path. Conversely, when an enough positive bias is applied, the Ga–O bonds in the switching layer can be broken by energetic electrons and further induce the re-formation of oxygen vacancies, as shown in Fig. 4(b).

In order to investigate the formation of the GaO_x film, X-ray photoelectron spectroscopy (XPS) analysis was performed. Fig. 5(a) and (b) shows the XPS analysis of O 1s (529.5 eV) [24]. Fig. 5 shows the composition ratio of O bonding to Ga $3d_{5/2}$ bonding in samples A and B is 1:1.07. This result indicates that the oxygen concentration of the GaO_x layer in sample B is indeed increased by sputtering in ambient Ar/O_2. Fig. 5(c) and (d) shows the XPS analysis of Ga $3d_{5/2}$. Using the Lorentzian–Gaussian functions analysis method, two peaks are present in both samples for the Ga $3d_{5/2}$ analysis. In Fig. 5(c) and (d), those peaks are verified to be Ga–O bonding (19.2 eV) and Ga–Ga bonding (18.2 eV) [24]. In order to investigate the influence of the additional oxygen atoms for the gallium oxide film, the composition of Ga $3d_{5/2}$ bonding was analysis. The composition ratio of the resistive switching layers can be identified by calculating the peak areas in the XPS analysis, with results indicating that, in comparison to sample A, the composition ratio of Ga–O bonding to Ga–Ga bonding increases in sample B. The additional oxygen atoms in sample B enhance the oxidation of Ga atoms, leading to the decreasing number of defects in the gallium oxide film. This analysis indicates the switching behavior of sample B is more stable because the additional oxygen can reduce the defects in the gallium oxide and decrease the distribution of conduction paths, as shown in the inset of Fig. 2.

In addition, as noted before, Fig. 3(b) shows that the conduction mechanism of HRS is dominated by the Schottky emission. The thickness of the switching layer is defined as effective thickness (d_{eff}), as shown in Fig. 4(b), and can be estimated from the Schottky emission equation: $J = AT^2 \exp\left[\frac{-q\left(\varphi_B - \sqrt{qV/4\pi\varepsilon_i d_{eff}}\right)}{kT}\right]$. The effective thickness can be estimated from the slope value $\frac{q}{kT}\sqrt{\frac{q}{4\pi\varepsilon_i d_{eff}}}$ in the plot of $\ln\left(\frac{J}{T^2}\right)$ versus $\sqrt{V}$. The k, ε_i and d_{eff} are the Boltzmann constant, permittivity and effective thickness of the resistive switching layer, respectively. The slopes of samples A and B are extracted to be 8.01 and 7.53, as shown in Fig. 6 and in Fig. 3(b). The estimated d_{eff} of sample B is about 2.53 nm, larger than that of sample A (2.23 nm). This result indicates that the oxygen-rich composition of sample B can provide sufficient oxygen ions to re-combine with the oxygen vacancies among the switching layer. Hence, the effective thickness of sample B is larger than that of sample A.

Fig. 7(a) shows the endurance over 10^4 cycles. When applying a +1.2 V with a 400 ns pulse width, the resistance state is switched from HRS to LRS. Conversely, the resistance state is switched from LRS to HRS by the −1.6 V pulse with a 600 ns pulse width. The obtained results reveal that both samples A and B can withstand at least 10^4 cycles and still retain approximately 1.5 orders in their respective resistance ratios. For the retention characteristics, after the 10^4 cycle endurance test, the LRS and HRS for both samples retains stable without degradation longer than 10^4 s at 85 °C, as shown in Fig. 7(b).

4. Conclusion

In summary, we deposited a GaO_x insulator by sputtering a $Ga_{0.4}O_{0.6}$ target in ambient Ar (sample A), and in Ar/O_2 (sample B) in order to enhance the concentration of oxygen atoms. The resistance value of sample B is increased in HRS, because the additional O_2 gas can provide sufficient oxygen ions to re-combine the oxygen vacancies along the switching layer, and a larger effective thickness can be formed. Furthermore, the switching behavior of sample B becomes more stable by reducing the defects in the gallium oxide.

Acknowledgment

This work was performed at National Science Council Core Facilities Laboratory for Nano-Science and Nano-Technology in Kaohsiung–Pingtung area and was supported by the National Science Council of the Republic of China under contract nos. NSC 100-2120-M-110-003 and NSC-97-2112-M-110-009-MY3.

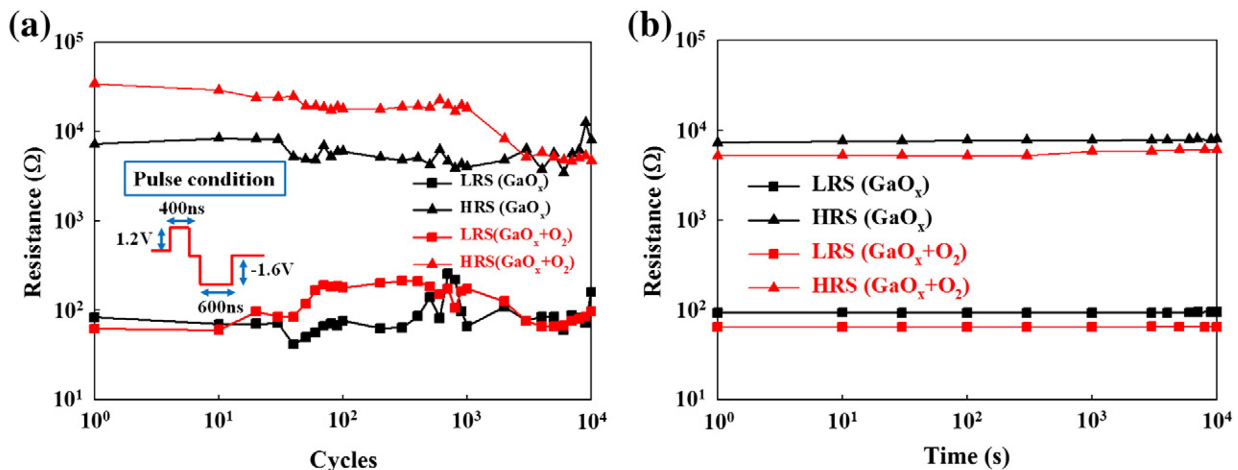

Fig. 7. (a) Endurance for 10^4 cycles as tested by AC sweeping, and (b) the retention for 10^4 s at 85 °C.

References

[1] T.C. Chang, F.Y. Jian, S.C. Chen, Y.T. Tsai, Mater. Today 14 (2011) 608.
[2] F.M. Yang, T.C. Chang, P.T. Liu, U.S. Chen, P.H. Yeh, Y.C. Tu, J.Y. Lin, S.M. Sze, J.C. Lou, Appl. Phys. Lett. 90 (2007) 222104.
[3] F.M. Yang, T.C. Chang, P.T. Liu, P.H. Yeh, Y.C. Yu, J.Y. Lin, S.M. Sze, J.C. Lou, Appl. Phys. Lett. 90 (2007) 132102.
[4] W.R. Chen, T.C. Chang, P.T. Liu, J.L. Yeh, C.H. Tu, J.C. Lou, C.F. Yeh, C.Y. Chang, Appl. Phys. Lett. 91 (2007) 082103.
[5] T.C. Chen, T.C. Chang, F.Y. Jian, S.C. Chen, C.S. Lin, M.H. Lee, J.S. Chen, C.C. Shih, IEEE Electron. Device Lett. 30 (2009) 834.
[6] G. Asano, H. Morioka, H. Funakubo, Appl. Phys. Lett. 83 (2003) 5506.
[7] A. Ney, J.S. Harris Jr., Appl. Phys. Lett. 86 (2005) 013502.
[8] T.C. Chong, L.P. Shi, R. Zhao, P.K. Tan, J.M. Li, H.K. Lee, X.S. Miao, A.Y. Du, C.H. Tung, Appl. Phys. Lett. 88 (2006) 122114.
[9] Y.T. Tsai, T.C. Chang, W.L. Huang, C.W. Huang, Y.E. Syu, S.C. Chen, S.M. Sze, M.J. Tsai, T.Y. Tseng, Appl. Phys. Lett. 99 (2011) 092106.
[10] L.W. Feng, C.Y. Chang, Y.F. Chang, W.R. Chen, S.Y. Wang, P.W. Chiang, T.C. Chang, Appl. Phys. Lett. 96 (2010) 052111.
[11] S.C. Chen, T.C. Chang, S.Y. Chen, C.W. Chen, S.C. Chen, S.M. Sze, M.J. Tsai, M.J. Kao, F.S. Yeh, Solid-State Electron. 62 (2011) 40.
[12] H.Y. Lee, P.S. Chen, T.Y. Wu, C.C. Wang, P.J. Tzeng, C.H. Lin, F. Chen, M.J. Tsai, C. Lien, Appl. Phys. Lett. 92 (2008) 142911.
[13] P.C. Yang, T.C. Chang, S.C. Chen, Y.S. Lin, H.C. Huang, D.S. Gan, Electrochem. Solid-State Lett. 14 (2011) H93.
[14] K.C. Chang, T.M. Tsai, T.C. Chang, Y.E. Syu, C.C. Wang, S.L. Chuang, C.H. Li, D.S. Gan, S.M. Sze, Appl. Phys. Lett. 99 (2011) 263501.
[15] K.M. Kim, B.J. Choi, B.W. Koo, S. Choi, D.S. Jeong, C.S. Hwang, Electrochem. Solid-State Lett. 9 (2006) G343.
[16] L.P. Ma, J. Liu, Y. Yang, Appl. Phys. Lett. 80 (2002) 2997.
[17] Y.E. Syu, T.C. Chang, T.M. Tsai, Y.C. Hung, K.C. Chang, M.J. Tsai, M.J. Kao, S.M. Sze, IEEE Electron Device Lett. 32 (2011) 545.
[18] L.W. Feng, Y.F. Chang, C.Y. Chang, T.C. Chang, S.Y. Wang, P.W. Chiang, C.C. Lin, S.C. Chen, S.C. Chen, Thin Solid Films 519 (2010) 1536.
[19] H. Shima, F. Takano, H. Muramatsu, H. Akinaga, I.H. Inoue, H. Takagi, Appl. Phys. Lett. 92 (2008) 043510.
[20] K.M. Kim, B.J. Choi, C.S. Hwang, Appl. Phys. Lett. 90 (2007) 242906.
[21] K. Jung, J. Choi, Y. Kim, H. Lm, S. Seo, R. Jung, D.C. Kim, J.S. Kim, B.H. Park, J.P. Hong, J. Appl. Phys. 103 (2008) 034504.
[22] M. Liu, Z. Abid, W. Wang, X. He, Q. Liu, W. Guan, Appl. Phys. Lett. 94 (2009) 233106.
[23] X. Gao, Y. Xia, J. Ji, H. Xu, Y. Sum, H. Li, C. Yang, H. Guo, J. Yin, Z. Liu, Appl. Phys. Lett. 97 (2010) 193501.
[24] J. Massies, J.P. Contour, J. Appl. Phys. 58 (1985) 806.